FISEVIER

Contents lists available at ScienceDirect

# Biosensors and Bioelectronics

journal homepage: www.elsevier.com/locate/bios



# A smartphone-based system for fluorescence polarization assays

Zijian Zhao<sup>a</sup>, Le Wei<sup>a</sup>, Mingfeng Cao<sup>b</sup>, Meng Lu<sup>a,c,\*</sup>

- <sup>a</sup> Department of Electrical and Computer Engineering, Iowa State University, Ames, IA 50011, United States
- <sup>b</sup> Department of Chemical and Biomolecule Engineering, Iowa State University, Ames, IA 50011, United States
- <sup>c</sup> Department of Mechanical Engineering, Iowa State University, Ames, IA 500110, United States



Keywords: Fluorescence polarization assay Immunoassay Smartphone Mobile sensor

#### ABSTRACT

This paper demonstrates the use of a smartphone-based sensor for fluorescence polarization (FP) analysis of biomolecules. The FP detection can rapidly sense ligand-analyte bindings by measuring molecule mobility, and thus, FP-based assays have been widely used for rapid diagnostics in clinics. Here, we implemented the FP detection apparatus using a 3D-printed compact holder and the built-in camera of a smartphone. The system offers accurate measurements of the degree of polarization by simultaneously detecting the fluorescence intensities parallel and perpendicular to the polarization of the excitation. The fluorescence signal of the sample is excited by a laser or light-emitting diode and separated by a polarization beam cube depending on the polarization. Parallel and perpendicular polarized emissions are projected onto two different regions of the sensor chip in the smartphone camera. A custom software app was developed to count the average intensity in the areas of interest and compute the degree of polarization. We validated the system by measuring the polarization of dye molecules dissolved in solutions with different viscosities. As an example of biomolecule sensing, a competitive FP immunoassay of Prostaglandin  $\rm E_2$  was demonstrated using the developed system and exhibited the limit of detection of 1.57 ng/mL. The smartphone-based FP assay platform can also be implemented for the detection of toxins, disease biomarkers, and pathogens in resource-limited settings.

# 1. Introduction

Fluorescence polarization (FP) interrogates the polarization of light emitted by fluorophores, which are excited by a linearly polarized excitation (Ameloot et al., 2013; Jameson and Ross, 2010; Lakowicz, 2006). Since fluorophores are free to rotate in solution, the polarization of fluorescence emission within the fluorescence lifetime can point at a direction that differs from the polarization of the excitation light. The change of FP depends on the molecule's rotational speed and is associated with the solution's viscosity, temperature, and the size of fluorescent molecules. In particular, the size-dependent feature has been utilized to develop FP immunoassays (FPIAs) (Duckworth and Aldrich, 2010; Flotow et al., 2002; Hall et al., 2016; Lea and Simeonov, 2011; Lucero et al., 2003). Most FPIAs detect the change of FP caused by the binding of fluorophore bound ligand to the analyte of interest. As a homogenous assay, the FPIA eliminates multiple washing steps and only requires simple sample preparation and signal readout (Jameson and Ross, 2010). Thus, the FPIA is suitable for the rapid detection of chemicals and biomolecules in resource-limited settings. Currently, expensive laboratory instruments are needed to measure FP signals. There is strong demand in using low-cost, compact, and portable systems to replace laboratory-based instruments.

Recently, smartphones, in conjunction with portable accessories, have been exploited for the *in-vitro* molecular diagnostics applications that have previously been available only to well-trained technicians using expensive analytical instruments (Hussain et al., 2017; Ludwig et al., 2015; Roda et al., 2016; Vashist et al., 2014; Xu et al., 2015; Zhang et al., 2015). For example, smartphone cameras have been adopted for several colorimetric detection assays, such as enzymelinked immunosorbent assay, lateral flow immunoassay, and nanoparticle-based homogenous assays (Berg et al., 2015; Guler et al., 2017; Long et al., 2014; Ludwig et al., 2015; Wang et al., 2017, 2016). Attached to a compact spectrum analyzer, smartphones can be turned into compact readers for Raman spectroscopy and reflectometric label-free biosensors (Ayas et al., 2014; Cetin et al., 2014; Dutta et al., 2014; Gallegos et al., 2013; Liu et al., 2018). Furthermore, smartphone-based fluorescence detectors have been demonstrated for fluorescence-based DNA and protein assays (Chen et al., 2017; Damhorst et al., 2015; Kuhnemund et al., 2017; Ludwig et al., 2015). These recent developments have been successfully implemented for pathogen detection, toxin detection, and disease diagnosis (Koydemir et al., 2015; Priye et al., 2017; Quesada-Gonzalez and Merkoci, 2017; Wei et al., 2013).

<sup>\*</sup>Corresponding author at: Department of Electrical and Computer Engineering, Iowa State University, Ames, IA 50011, United States. E-mail address: menglu@iastate.edu (M. Lu).

Using a smartphone, citizens with minimum training can carry out assays and thus facilitate the goal of point-of-need tests for *in-vitro* diagnosis.

This paper demonstrates a smartphone-based FP detector that is capable of measuring the degree of polarization and thus detecting biomolecules. To obtain a compact FP detector, we implement a novel optical design that integrates a 3D printed housing and off-the-shelf optical components. The FP detector interfaces with smartphones through the built-in camera and a customized application (app). The compact FP detector can measure the degree of polarization with the performance comparable to a commercial laboratory fluorescence plate reader. The smartphone-based FP detection can be applied to most existing FPIAs. As an example, we demonstrate the quantification of a drug compound using a competitive FPIA. By combining the rapid, nowash, and low-cost features of the FPIA and detector, the smartphone-based FPIA plateform offers a promissing solution for affordable bed-side diagnostics.

#### 2. Material and methods

# 2.1. Materials and reagents

Rhodamine 6G (R6G) and Coumarin 540 A were purchased from Exciton (Oakley Inc. West Chester, OH, USA). Methanol, phosphate buffered saline (PBS), and glycerol were obtained from Sigma-Aldrich (St. Louis, MO, USA). Prostaglandin E2 (PGE $_2$ ) FPIA kit (Catalog # ADI-920-001) was purchased from Enzo Life Sciences Inc. (Farmingdale, NY, USA). The FPIA kit contains a monoclonal PGE $_2$  antibody, assay buffers, fluorescein-conjugated PGE $_2$ , and PGE $_2$  standard sample.

# 2.2. FP detection apparatus

The underlying principle of FP analysis is illustrated in Fig. 1(a), where the fluorescent molecules are excited by a linearly polarized light, and then the polarization of their fluorescent emission is analyzed. For molecules that rotate slowly with regard to the fluoresce lifetime, the emission is polarized. In contrast, the emission of fast

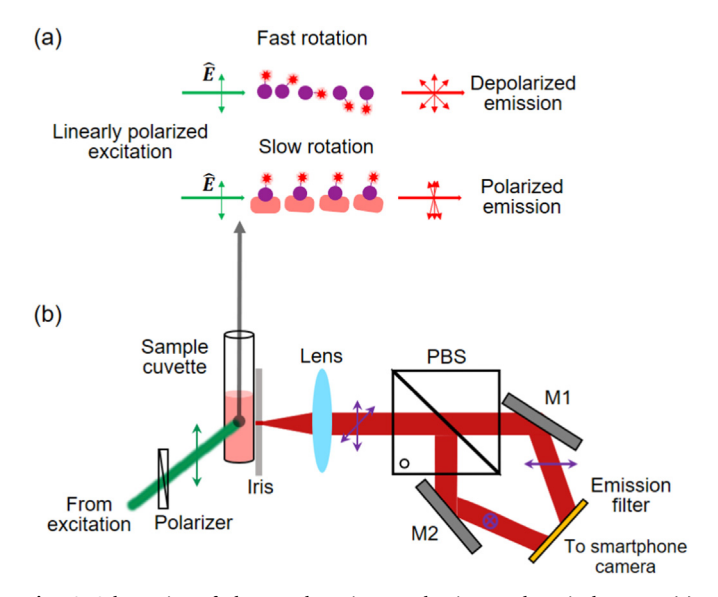


**Fig. 1.** Schematics of the FP detection mechanism and optical setup. (a) Illustration of the FP assay. The fluorescence molecules are excited by a linearly polarized laser and the polarization state of the emission correlates to the rotation speed of the molecules. The binding with target molecules slows down the rotation and results in a more polarized emission. (b) The smartphone-based FP system setup consisting of a linearly polarized excitation, sample cuvette, iris, collection lens, polarizing beam splitter, two mirrors, emission filter, and smartphone camera.

rotating molecules become depolarized. The design of a compact FP analyzer (Fig. 1(b)) can be implemented to determine the degree of polarization.

The FP detection apparatus consists of a smartphone (HTC One M8 running Android 6.0) and a 3D-printed housing that contains optical components and can be attached to the rear camera of the smartphone. The housing of the FP detector was designed using SOLIDWORKS (Dassault Systems Inc., MA, USA) as shown in Fig. 2(a). The housing was printed by Shapeways Inc. (NY, USA) using acrylic with a black finish. Fig. 2(b) shows the 3D-printed housing with all optical components including an excitation light source (DJ532-10 or L462P1400MM; Thorlabs Inc., NJ, USA), a collimation lens (LJ1402L1: Thorlabs Inc.), a linear polarizer (40–990; Edmund Optics Inc., NJ, USA), a plano-convex lens (LA154-A; Thorlabs Inc.), a polarizing beam splitter (49-001; Edmund Optics Inc.), two mirrors (43-790; Edmund Optics Inc.), and a bandpass filter (1005190B and FF02-485/20-25, Semrock Inc). The black surface finish and the cover prevent stray light from reaching the camera. In this work, a microfluorescence cuvette with the light path length of 3 mm (Type 507, FireflySci Inc.) was used to hold samples. The cuvette can be inserted into the housing to perform FP assays. The overall size of the fabricated housing is  $98 \text{ mm} \times 60 \text{ mm} \times 58 \text{ mm}$ .

To design the FP detection optics, we utilized an optical design software (LightTools 8.5, Synopsys Inc.) to simulate and optimize the fluorescence imaging system that can measure two different polarizations simultaneously. In the assembled system, the collimation lens (focal length = 15 mm) is placed in front of the blue laser diode ( $\lambda = 462 \, \text{nm}$  and  $P_{\text{max}} = 1400 \, \text{mW}$ ) or the diode-pumped green laser source ( $\lambda = 532 \, \text{nm}$  and  $P_{\text{max}} = 40 \, \text{mW}$ ) to create a collimated excitation beam with the beam diameter of 2 mm. The excitation source can be easily installed and changed at the input port and are powered by the battery stored in the battery compartment as shown in Fig. 2(a). The collimated laser beam is vertically polarized with the electric field along the z-axis (Fig. 1(b)). During the 3D printing process, a pinhole (diameter of 1 mm) was created on the thin-wall against the sample cuvette. The position of the pinhole is aligned at the center point of the excited volume inside the cuvette. A projection lens (focal length = 11 mm) collects fluorescent light emerging from the excited volume passing through the pinhole. Then, the fluorescent light is split into two beams depending on the polarization using the polarizing beam splitter cube, as shown in Fig. 1(b). The vertical and horizontal polarizations  $(I_{//}$  and  $I_{\perp})$  are reflected by the mirror, which is oriented at an angle of 30° to the light path. To enable the analysis of the degree of polarization, two beams, representing  $I_{//}$  and  $I_{\perp}$  emissions, are collected by the rear camera of the smartphone. As illustrated in Fig. S1, the smartphone can be attached to the 3D-printed housing with its camera behind the emission filter. The emission filter, selected according to the fluorophore, can be inserted in the filter slot in front of the smartphone camera. The camera needs aligned to the fluorescent beams to image the beams at two different locations on the internal CMOS sensor, which is sensitive to visible light from 400 nm to 700 nm. The width of each fluorescent imaging spot is ~25 pixels.

# 2.3. Android app for image processing

The Android app was developed to capture images from the smartphone camera and calculate the degree of fluorescence polarization. The app functions as a graphic user interface that allows users to read and record assay results instantaneously. Images acquired from the CMOS sensor consists of  $2592 \times 1936$  pixels (20 megapixels), and each pixel represents a 24-bit RGB color. As shown in Fig. S2 of the Supporting information, the app can identify the spots of vertically and horizontally polarized fluorescence and calculate the FP-value. For the sample with a low degree of polarization, the intensities of the spots are close, and *vice versa*. For both vertically and horizontally polarized spots, the intensities of red, green, and blue components are extracted, averaged, and displayed on the screen. The intensity of each channel

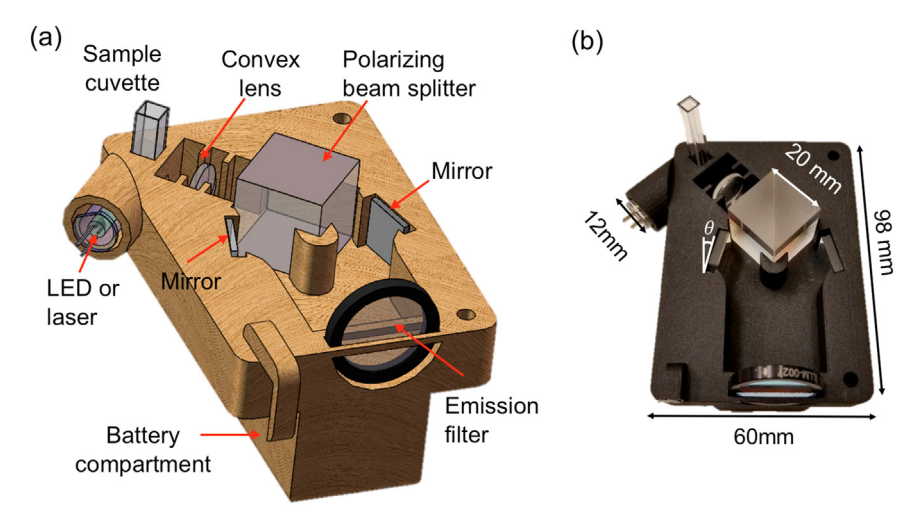


Fig. 2. Diagram and photograph of the FP hardware. (a) Schematic design illustrating the housing and optics inside the FP detector. (b) Photograph of the 3D-printed housing and installed optical components. The total weight is less than 175 g. The cover part of the housing is not shown.

ranges from 0 to 255. Since the fluorescence emissions usually fall within a given spectral band, the app calculates the FP-value based on the color channel specified by users.

#### 2.4. Fluorescence anisotropic tests

The smartphone-based FP detection system was tested using two proof-of-concept fluorescence anisotropic experiments. The degree of polarization of two fluorescence dyes (Rhodamine 6 G and Coumarin 540 A) dissolved in solutions with different viscosities was characterized. The fluorescent dyes were dissolved in methanol with the concentration of 0.01 mg/mL for both Rhodamine 6 G and Coumarin 540 A samples. Glycerol was added in the dye solutions to adjust their viscosities. A series of samples with different amounts of glycerol, from 0% to 83% (v/v %) were prepared. Based on the volume ratio of the mixtures, the sample viscosity can be calculated (Cheng, 2008; Volk and Kahler, 2018). These samples were measured to determine the fluorescence intensities ( $I_{1/l}$  and  $I_{\perp}$ ). The FP-value can be calculated using:  $FP = \frac{I_{1/l} - I_{\perp}}{I_{1/l} + I_{\perp}}$  (Ameloot et al., 2013). The degree of polarization of the samples was also measured using a laboratory desktop fluorimeter (Synergy 2 Multi-Mode Microplate Reader, BioTek).

# 2.5. FPIA assay for PGE2

As an example, PGE<sub>2</sub> was chosen as the analyte to demonstrate the quantitative FP analysis of biomarker using the smartphone platform. The reagents of PGE2 detection assay were provided in the FPIA assay kit. The assay was performed in the cuvette in a competitive manner. The first step is to add the PGE<sub>2</sub> analyte with a volume of 50 μL into the cuvette. Then, a  $25\,\mu L$  fluorescein-conjugated PGE<sub>2</sub> ( $10\,\mu g/mL$ ) was pipetted into the same cuvette and mixed with the unlabeled analyte. The mixture was incubated with a 25 µL of PGE2 specific antibody (10 µg/mL) for 30 min. And as a competitive immunoassay, the unlabeled analyte in the sample competes with the fluorescein-labeled PGE2 to bind the PGE2 antibody. Hence, the amount of labeled and unbound PGE2 is proportional to the amount of analyte in the sample. After the incubation, the cuvette was inserted into the dongle and the FP results were read using the smartphone. The emission of fluorescein was excited using the blue laser diode and imaged through the green bandpass filter.

#### 3. Results and discussion

# 3.1. Fluorescence anisotropy measurement of dyes

As a proof-of-concept experiment, we measured the FP-values of two organic dyes (Rhodamine 6 G (R6G) and Coumarine 540) dissolved in methanol solutions with different viscosities. A sample with a high viscosity should exhibit a high degree of polarization since the dye molecule rotation becomes slow. To adjust the sample viscosity, we added glycerol into the methanol solutions. At room temperature, the viscosities of glycerol and methanol are 1.41 Pa s and 0.57 mPa s, respectively. It is possible to control the sample viscosity by mixing glycerol and methanol at a desired percentage. The R6G and Coumarine 540 dyes have different absorption and emission signatures. The Android app and FP detector were slightly modified to measure the FP-values of both dyes. The details of the experiment, smartphone setup, and results are discussed as follows.

# 3.1.1. Fluorescence anisotropy measurement of R6G

The R6G dye is a highly efficient fluorophore with the absorption maximum and emission maximum located at approximately 530 nm and 575 nm, respectively. To measure the fluorescence emission of R6G, we installed the diode-pumped green laser ( $\lambda_{\rm ex}=532\,{\rm nm}$ ) and the bandpass filter (560 nm <  $\lambda_{\rm ex}<592\,{\rm nm}$ ) in the 3D-printed holder. Since the main portion of the R6G emission locates in yellow and red wavelengths, the Andriod app determines the spot intensities with only the red channel of acquired RGB images. To prepare the samples, we dissolved R6G in methanol at the concentration of 0.01 mg/mL and mixed the R6G-methanol solution with glycerol. For this experiment, 13 R6G samples were prepared to generate a series of viscosities with the glycerol concentration ranging from 0% to 83.33% (v/v,%). The corresponding viscosities of the samples are from 0.89 mPa s to 97 mPa s.

The fluorescence images of the samples with glycerol concentrations of 0%, 40%, and 80% are shown in Fig. 3(a) from top to bottom. The exposure time was kept at 10 ms during the experiments. The red channel was extracted from the RGB images, and the averaged intensity in each fluorescent spot was calculated. For each concentration, the left and right spots represent the vertically and parallelly polarized fluorescence emissions, respectively. The sample with a high concentration exhibits a more significant difference with regards to the spot intensity. To compare the  $I_{I/I}$  and  $I_{\perp}$  quantitatively, the intensity profiles along the dashed lines across both fluorescent spots in Fig. 3(a) are compared in Fig. 3(b). The sample without glycerol (red curve) shows nearly equivalent emissions for both polarizations. The increase of glycerol concertation results in the uneven emissions as shown in the yellow and

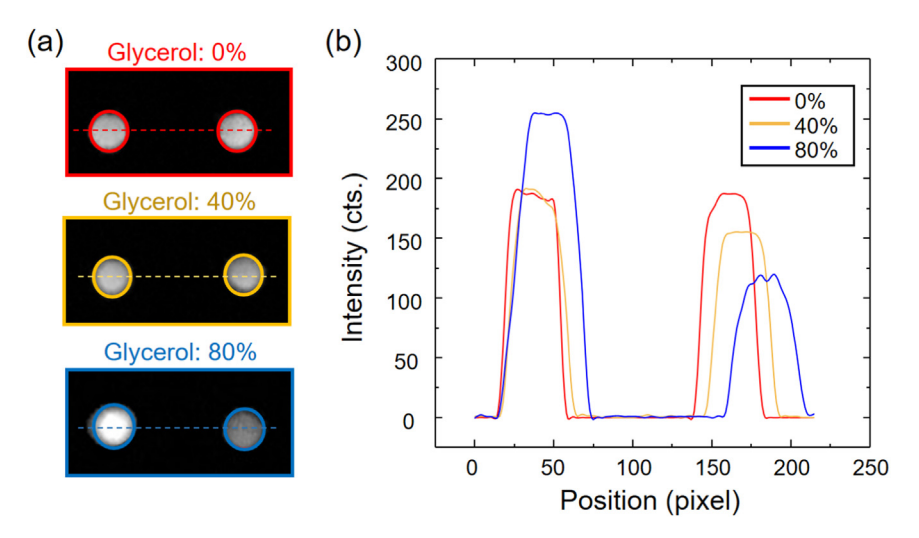


**Fig. 3.** Analysis of FP-values for samples with different viscosities. (a) Beam spots for vertical (left spot) and horizontal (right spot) polarizations for the R6G solutions mixed with glycerol at the v/v ratio of 0%, 40%, and 80%, respectively. Only the red channels of the beam spots are shown. (b) Intensity profiles along the dashed lines shown in the images of beam spots. The beam intensities are plotted as a function of the CCD pixel. (For interpretation of the references to color in this figure legend, the reader is referred to the web version of this article).

blue curves. The FP-value reflects the degree of difference between the vertically and parallelly polarized emissions. Based on the averaged emission intensity in the left and right spots, the FP-values of the samples with 0%, 40%, and 80% glycerol are 0.08, 82, and 308.42 milli-polarization (mP), respectively.

The semi-log graphs in Fig. 4 are plotted with a logarithmic scale on the x-axis representing the sample viscosity and a linear scale on the yaxis representing the FP-value with the unit of mP. The results in Fig. 4(a) were measured using the smartphone-based FP detector. Measured data was fitted using the exponential function as shown by the red curve. The curve follows an exponential trend, and the polarization value reaches saturation when the sample viscosity is over 0.04 Pas. The linear response region is from 0.003 Pas to 0.041 Pas. For each viscosity, three replicated samples (n = 3) were measured and the coefficient of variation (C.V.) was calculated using C.V. =  $\sigma/\mu$ , where  $\sigma$  and  $\mu$  represent the standard deviation and mean values of the FP-values, respectively. To validate the smartphone-based system, we also measured the same samples using a commercial fluorescent plate reader (Synergy 2, BioTek). The results obtained by the benchtop reader are plotted in Fig. 4(b). The response curves in Fig. 4(a) and (b) match well.

# 3.1.2. Fluorescence anisotropy measure of Coumarin 540 The smartphone-based system can be implemented to measure FP

signals emitted by many fluorophores. In addition to R6G, Coumarin 540 is a common organic dye, which has been widely used as the optical gain medium in dye lasers. The absorption and emission bands of Coumarin 540 locate at approximately 460 nm and 550 nm, respectively. The FP detector only needs to be slightly modified to measure the FP signals emitted by Coumarin 540. We replaced the green laser with a blue LED ( $\lambda_{\rm ex}=485\,{\rm nm}$ ) and changed the bandpass filter to one with an emission band of 465 nm <  $\lambda_{\rm ex}<495\,{\rm nm}$ . Since the main portion of the Coumarin 540 emission locates in the green region, the app calculates the  $I_{I/I}$  and  $I_{\perp}$  values based on the green channel of acquired RGB images.

Similar to the measurement of R6G samples, we prepared 13 samples with Coumarin 540 dissolved in methanol and different concentrations of glycerol. For each viscosity, three replicated samples were measured to calculate the C.V. numbers. The Coumarin 540 dye was dissolved in methanol at the concentration of 0.01 mg/mL. To generate the series of viscosities, we mixed the Coumarin 540 solution with the glycerol. The glycerol concentration and solution viscosity range from 0% to 83.3% (v/v,%) and from 0.89 mPas to 97 mPas, respectively. The semi-log plot in Fig. 5 shows the measured polarization value as a function of sample viscosity. The FP curve of Coumarin 540 follows the same trend as the R6G test shown in Fig. 5. The results of the FP analysis of organic dye solutions with different viscosities demonstrates the feasibility of using the smartphone system for FP-

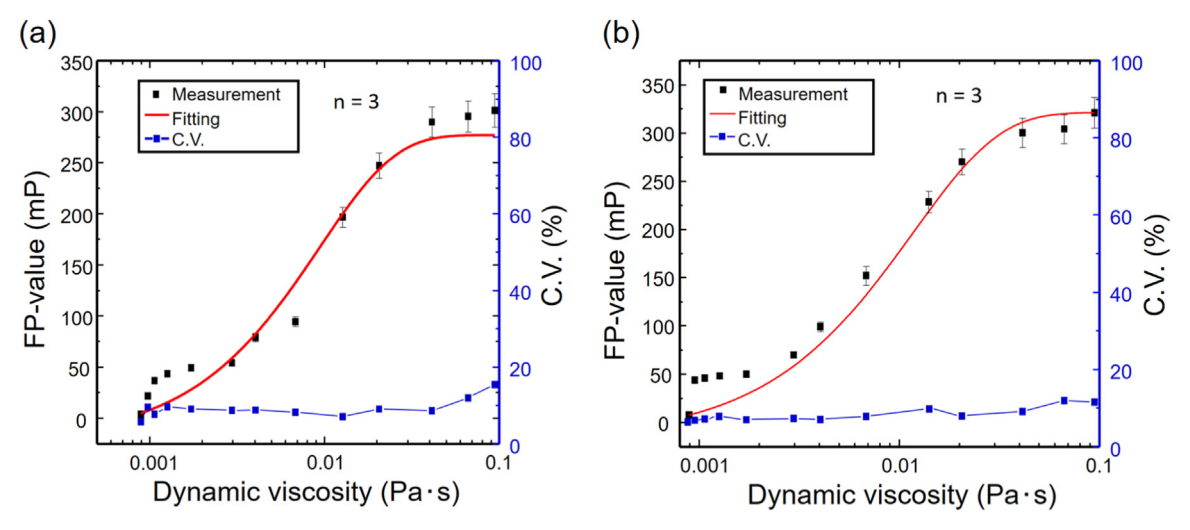


**Fig. 4.** FP-values plotted as a function of the R6G sample viscosity. The FP response curve measured using the smartphone-based FP detector (a) and the benchtop plate reader (b). The FP-values and C.V. numbers are shown by the left and right axes, respectively. The FP-values are fitted using exponential functions of  $y = -299e^{-106.4x} + 277$  and  $y = -338e^{-84.7x} + 321$  in (a) and (b), respectively. The error bar represents the standard deviation of the replicated samples.

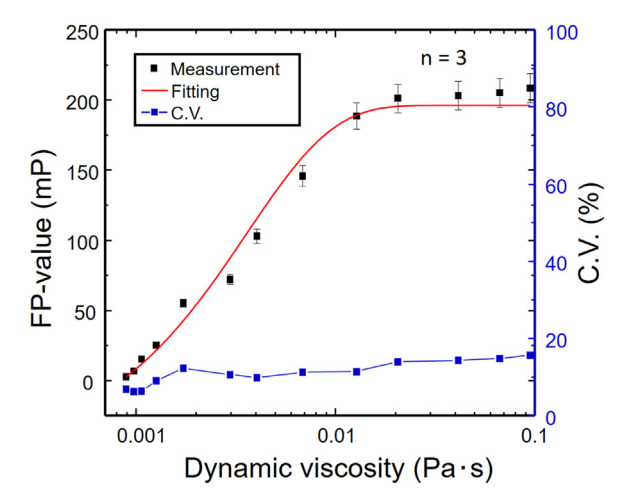


**Fig. 5.** FP-values plotted as a function of the viscosity of Coumarin 540 solutions. The FP analysis of Coumarin 540 emission was performed using the green channel of the images acquired by the smartphone's CCD sensor. The FP-values and C.V. numbers are shown by the left and right axes, respectively. The measured result was fitted using an exponential curve  $(y = -248e^{-277.8x} + 196.4)$ .

based analysis.

# 3.2. FPIA detection of PGE2

To determine the performance of the smartphone-based system for biomolecule analysis, the detection of  $PGE_2$  was performed using a competitive FP immunoassay.  $PGE_2$  is a bioactive lipid that is relevant to a wide range of biological effects. For example,  $PGE_2$  can be released by blood vessel walls in response to infection, inflammation, or cancer (Flower and Blackwell, 1976; Moncada and Vane, 1978). Here, the detection for  $PGE_2$  is performed in the manner of a competitive homogeneous immunoassay, where analyte (unlabeled  $PGE_2$ ) competes with labeled  $PGE_2$  molecules to bind the  $PGE_2$ -specific antibody. The binding of a fluorescein-conjugated  $PGE_2$  molecule to its antibody results in a slower rotation and consequently an increased FP-value. The presence of the analyte  $PGE_2$  competes with the labeled  $PGE_2$  and results in a smaller change of the FP-value. Therefore, the FP-value should

be inversely proportional to the amount of analyte in the sample. The protocol of the competitive FPIA assay for  $PGE_2$  is summarized in Fig. 6(a).

To generate a titration curve for the analysis of PGE2, we prepared PGE<sub>2</sub> samples at a series of seven concentrations ranging from 1.64 ng/ mL to 100 ng/mL, with 2.5-fold dilutions and a reference sample without PGE2. For each PGE2 concentration, eight replicated samples were prepared and measured. We measured the signal of a sample without the fluorescein-conjugated PGE2 and used it as the background signal. The background signal was subtracted from the imaged fluorescent spots. The FP-values of all these samples were calculated and shown in Fig. 6(b) as the dose-response curve. The measured curve correlates well with the results provided by the manufacture of the PGE2 FPIA kit (Enzo Life Sciences Inc, 2018). The limit of detection (LOD) of the FPIA was calculated based on the FP-value that represents zero analyte concentration plus the three times of the standard deviation  $(FP_{LOD} = FP_0 + 3\sigma)$  (Taylor et al., 2001). For the detection of PGE<sub>2</sub>, the LOD value is 1.57 ng/mL (Fig. 6(b)). It is worth noting that the proof-of-concept FPIA experiment used the PGE2 samples dissolved in PBS buffer without interfering molecules. Because of the limited selectivity of immunoassays, the LOD value may vary when PGE2 molecules are in a complex buffer, such as blood or urine, Here, we focus on the demonstration of the smartphone-based FP detector, rather than a particular FPIA detection.

# 4. Conclusions

This paper demonstrates a portable FP detection system that exploits the smartphone hardware to perform FPIAs. The FP detector, consisting of a 3D-printed housing and off-the-shelf optical components, can be attached to smartphones for a rapid FP analysis. The FP detector was prototyped with the total cost of \$300 and weight of 175 g. We also developed a mobile app that functions as the user interface to facilitate the tests. Using two proof-of-concept experiments for red and green fluorescent dyes, we showed the system is capable of measuring FP states of the dye molecules and is identical to a commercial benchtop microplate reader. Furthermore, the smartphone-based FPIA was implemented to detect PGE<sub>2</sub> with a detection limit of 1.57 ng/mL. Owing to the benefits of portability and low cost, the smartphone-based FP detector can be adopted as a point-of-care testing tool for a variety of chemicals and biomolecules, such as biomarkers, drug compounds,

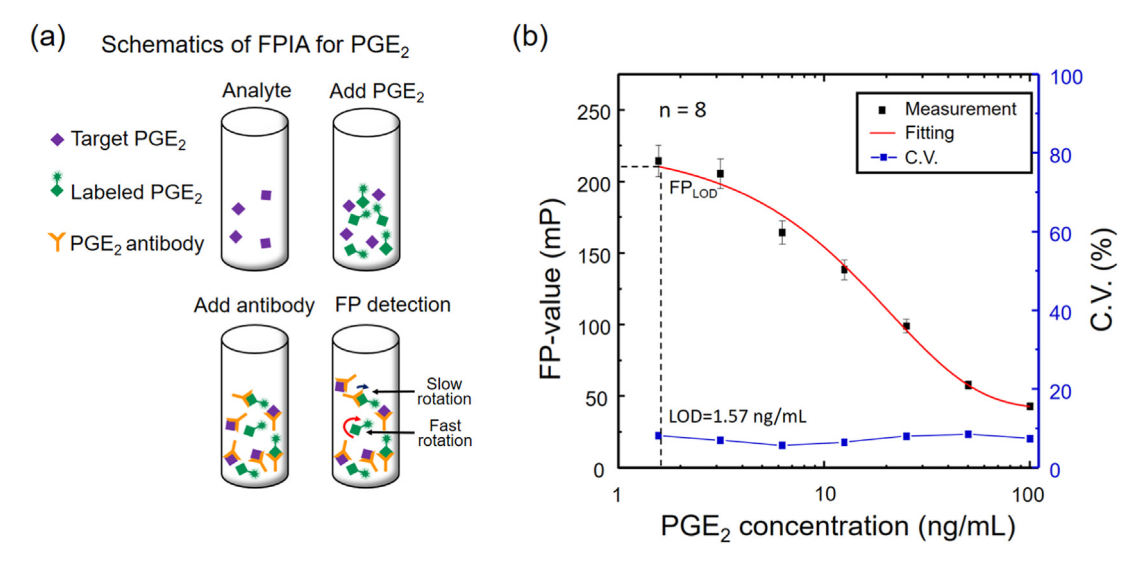


Fig. 6. (a) Major steps of the FPIA detection assay for PGE<sub>2</sub>. As a competitive assay, the analyte is mixed with the fluorophore-labeled PGE<sub>2</sub> molecules and incubated with the PGE<sub>2</sub> antibody. The presence of PGE<sub>2</sub> consumes the antibody molecules and results in a higher number of the unbound, fast-rotation, and labeled PGE<sub>2</sub>. (b) Titration curve of PGE<sub>2</sub> with the FP-values measured using the smartphone-based FP detector. The left and right axes show the FP-values and C.V. numbers, respectively. The data points are fitted using an exponential curve ( $y = 182e^{-\frac{X-1.3}{20684}} + 41.5$ ) shown in red.

toxins, and metabolite products. For future work, we will explore the potentials in the following aspects. Firstly, a microfluidic chip will be integrated with the FP detector to enable multiplexed FP detections with minimized sample volume. The microfluidics chip will further reduce the assay time to meet the needs of rapid analysis for point-of-care testing. Secondly, we will add network connectivity to the mobile app in order to allow civilian users to share the FPIA results. Thirdly, the mobile FP technology in conjunction with FPIAs will be explored in potential fields, such as environmental monitoring and food safety in resource limited settings.

# CRediT authorship contribution statement

Zijian Zhao: Conceptualization, Methodology, Software, Validation, Formal analysis, Investigation, Data curation, Writing original draft, Visualization, Supervision. Le Wei: Methodology, Software, Formal analysis, Data curation, Writing original draft. Mingfeng Cao: Methodology, Investigation. Meng Lu: Conceptualization, Methodology, Resources, Writing original draft, Writing original draft, Writing original draft, Supervision, Project administration, Funding acquisition.

# Acknowledgments

This research was supported by the National Science Foundation under grant ECCS 16-53673, and the National Institute of Food and Agriculture under Award No. 2018-67021-27968. Any opinions, findings, and conclusions or recommendations expressed in this material are those of the author(s) and do not necessarily reflect the views of the National Science Foundation.

# Appendix A. Supporting information

Supplementary data associated with this article can be found in the online version at doi:10.1016/j.bios.2018.12.031.

# References

- Ameloot, M., VandeVen, M., Acuna, A.U., Valeur, B., 2013. Pure Appl. Chem. 85 (3), 589–608.
- Ayas, S., Cupallari, A., Ekiz, O.O., Kaya, Y., Dana, A., 2014. ACS Photonics 1 (1), 17–26.
   Berg, B., Cortazar, B., Tseng, D., Ozkan, H., Feng, S., Wei, Q.S., Chan, R.Y.L., Burbano, J., Farooqui, Q., Lewinski, M., Di Carlo, D., Garner, O.B., Ozcan, A., 2015. ACS Nano 9 (8) 7857–7866
- Cetin, A.E., Coskun, A.F., Galarreta, B.C., Huang, M., Herman, D., Ozcan, A., Altug, H.,

- 2014. Light Sci. Appl. 3 (1), e122.
- Chen, W.L., Yu, H.J., Sun, F., Ornob, A., Brisbin, R., Ganguli, A., Vemuri, V., Strzebonski, P., Cui, G.Z., Allen, K.J., Desai, S.A., Lin, W.R., Nash, D.M., Hirschberg, D.L., Brooks, I., Bashir, R., Cunningham, B.T., 2017. Anal. Chem. 89 (21), 11219–11226.
- Cheng, N.S., 2008. Ind. Eng. Chem. Res. 47 (9), 3285-3288.
- Damhorst, G.L., Duarte-Guevara, C., Chen, W., Ghonge, T., Cunningham, B.T., Bashir, R., 2015. Engineering 1 (3), 324–335.
- Duckworth, B.P., Aldrich, C.C., 2010. Anal. Biochem. 403 (1-2), 13-19.
- Dutta, S., Choudhury, A., Nath, P., 2014. IEEE Photon. Tech. Lett. 26 (6), 568–570. Flotow, H., Leong, C.Y., Buss, A.D., 2002. J. Biomol. Screen. 7 (4), 367–371.
- Flower, R.J., Blackwell, G.J., 1976. Biochem. Pharmacol. 25 (3), 285-291.
- Gallegos, D., Long, K.D., Yu, H., Clark, P.P., Lin, Y., George, S., Nath, P., Cunningham, B.T., 2013. Lab Chip 13 (11), 2124–2132.
- Guler, E., Sengel, T.Y., Gumus, Z.P., Arslan, M., Coskunol, H., Timur, S., Yagci, Y., 2017.
  Anal. Chem. 89 (18), 9629–9632.
- Hall, M.D., Yasgar, A., Peryea, T., Braisted, J.C., Jadhav, A., Simeonov, A., Coussens, N.P., 2016. Methods Appl. Fluoresc. 4 (2), 022001.
- Hussain, I., Das, M., Ahamad, K.U., Nath, P., 2017. Sens. Actuators B Chem. 239, 1042–1050.
- Jameson, D.M., Ross, J.A., 2010. Chem. Rev. 110 (5), 2685-2708.
- Koydemir, H.C., Gorocs, Z., Tseng, D., Cortazar, B., Feng, S., Chan, R.Y.L., Burbano, J., McLeod, E., Ozcan, A., 2015. Lab Chip 15, 1284–1293.
- Kuhnemund, M., Wei, Q.S., Darai, E., Wang, Y.J., Hernandez-Neuta, I., Yang, Z., Tseng, D., Ahlford, A., Mathot, L., Sjoblom, T., Ozcan, A., Nilsson, M., 2017. Nat. Commun. 8, 13913
- Lakowicz, J.R., 2006. Springer US, Boston, MA. https://doi.org/10.1007/978-0-387-46312-4
- Lea, W.A., Simeonov, A., 2011. Expert Opin. Drug Discov. 6 (1), 17-32.
- Liu, Q., Yuan, H., Liu, Y., Wang, J., Jing, Z., Peng, W., 2018. J. Biomed. Opt. 23 (4), 1–6.
  Long, K.D., Yu, H., Cunningham, B.T., 2014. Biomed. Opt. Express 5 (11), 3792–3806.
  Lucero, N.E., Escobar, G.I., Ayala, S.M., Paulo, P.S., Nielsen, K., 2003. J. Med. Microbiol. 52 (10), 883–887.
- Ludwig, S.K.J., Tokarski, C., Lang, S.N., van Ginkel, L.A., Zhu, H.Y., Ozcan, A., Nielen, M.W.F., 2015. PLoS One 10 (8), e0134360.
- Moncada, S., Vane, J.R., 1978. Pharmacol. Rev. 30 (3), 293-331.
- Priye, A., Bird, S.W., Light, Y.K., Ball, C.S., Negrete, O.A., Meagher, R.J., 2017. Sci. Rep. 7, 44778.
- Quesada-Gonzalez, D., Merkoci, A., 2017. Biosens. Bioelectron. 92, 549–562.
- Roda, A., Michelini, E., Zangheri, M., Di Fusco, M., Calabria, D., Simoni, P., 2016. Trends Anal. Chem. 79, 317–325.
- Taylor, J., Picelli, G., Harrison, D.J., 2001. Electrophoresis 22 (17), 3699–3708.
- Vashist, S.K., Mudanyali, O., Schneider, E.M., Zengerle, R., Ozcan, A., 2014. Anal. Bioanal. Chem. 406 (14), 3263–3277.
- Volk, A., Kahler, C.J., 2018. Exp. Fluids 59 (5), 59-75.
- Wang, L.J., Chang, Y.C., Sun, R.R., Li, L., 2017. Biosens. Bioelectron. 87, 686–692. Wang, Y., Liu, X.H., Chen, P., Tran, N.T., Zhang, J.L., Chia, W.S., Boujday, S., Liedberg, B.,
- Wang, Y., Liu, X.H., Chen, P., Iran, N.T., Zhang, J.L., Chia, W.S., Boujday, S., Liedberg, B. 2016. Analyst 141 (11), 3233–3238.
- Wei, Q.S., Qi, H.F., Luo, W., Tseng, D., Ki, S.J., Wan, Z., Gorocs, Z., Bentolila, L.A., Wu, T.T., Sun, R., Ozcan, A., 2013. ACS Nano 7 (10), 9147–9155.
- Xu, X.Y., Akay, A., Wei, H.L., Wang, S.Q., Pingguan-Murphy, B., Erlandsson, B.E., Li, X.J., Lee, W., Hu, J., Wang, L., Xu, F., 2015. Proc. IEEE 103 (2), 236–247.
- Enzo Life Sciences Inc, 2018. PGE $_2$  FPIA kit.  $\langle \text{http://www.enzolifesciences.com/ADI-920-001/pge2-fpia-kit/} \rangle$ .
- Zhang, D.M., Jiang, J., Chen, J.Y., Zhang, Q., Lu, Y.L., Yao, Y., Li, S., Liu, G.L., Liu, Q.J., 2015. Biosens. Bioelectron. 70, 81–88.